Resveratrol-Loaded Dissolving Microneedles: Fabrication and *in vitro* Evaluation

Banghuai Xing[1] Qian Luo[1] Tiantian Gan[1] Yi Jin[1] Jianfang Feng[1,2] Meng Cheng[3*] Liangxing Tu[1*]

[1] Division of Innovative Pharmaceutical Sciences, National Pharmaceutical Engineering Center for Solid Preparation in Chinese Herbal Medicine, Jiangxi University of Traditional Chinese Medicine, Nanchang, People's Republic of China
[2] Department of Pharmaceutical Sciences, School of Pharmacy, Guangxi University of Chinese Medicine, Nanning, People's Republic of China
[3] GCP Center, The Affiliated Hospital of Jiangxi University of Chinese Medicine, Nanchang, People's Republic of China

Address for correspondence Meng Cheng, PhD, The Affiliated Hospital of Jiangxi University of Chinese Medicine, 445 Bayi Avenue, Nanchang 330006, People's Republic of China (e-mail: cmjxzyy@126.com).

Liangxing Tu, PhD, National Pharmaceutical Engineering Center for Solid Preparation in Chinese Herbal Medicine, Jiangxi University of Traditional Chinese Medicine, 56 Yangming Road, Nanchang 330006, People's Republic of China (e-mail: tufrankie@163.com).

Pharmaceut Fronts 2024;6:e439–e448.

Abstract

Resveratrol (Res), an active ingredient derived from a multitude of plants, exhibits multiple pharmacological activities. However, its poor water solubility and low bioavailability present significant challenges to its clinical application. Our study aimed to improve the transdermal absorption of Res using dissolving microneedle (MN) technology, which could effectively overcome the stratum corneum barrier. Res-loaded dissolving microneedles (Res-MNs) were fabricated using polyvinyl pyrrolidone K90 (PVP K90) as the matrix material, and a two-step casting procedure was employed. The process was optimized using the Box–Behnken experimental design approach. The characteristics of Res-MNs *in vitro*, including morphology, solubility, safety evaluation, and skin permeation, were studied. The results showed that the optimum preparation conditions of Res-MNs were a centrifugation time of 10 minutes, a solvent concentration of 25%, and a prescription ratio (Res: matrix) of 0.375. The skin permeability of the Res-MNs was enhanced compared with Res suspension and Res gel. The cumulative release of Res-MNs *in vitro* was 75%, which was approximately 5 and 3 times that of the Res suspension group and Res gel group. These results suggest that dissolving MNs may represent a potential approach for enhancing the transdermal delivery of poorly absorbed drugs such as Res.

Keywords
- microneedle
- transdermal
- resveratrol
- absorption
- polyvinylpyrrolidone K90

Introduction

Resveratrol (Res) is a natural polyphenol extracted from *Polygonum cuspidatum*, grape, peanut, mulberry, and other plants.[1–4] Res exhibits extensive biological activities, including anticancer, anti-inflammatory, antioxidant, antiviral, and antineuralgic and heart protection.[5–10] Despite the proven therapeutic efficacy of Res in treating numerous diseases, several factors impede its optimal effectiveness. These include chemical instability, poor absorption through the biofilm, and low oral bioavailability due to first-pass metabolism and rapid elimination.[11–14] Moreover, Res is classified as a Biopharmaceutics Classification System II drug, exhibiting low aqueous solubility (< 0.05 mg/mL) and

received
November 22, 2023
accepted
September 24, 2024
article published online
November 8, 2024

DOI https://doi.org/10.1055/s-0044-1791832.
ISSN 2628-5088.

Georg Thieme Verlag KG, Rüdigerstraße 14, 70469 Stuttgart, Germany

high permeability.[15] Consequently, the appropriate route of administration of Res is a crucial consideration.

Transdermal drug delivery represents an ideal drug administration method, offering the potential to maintain a constant blood concentration, reduce adverse reactions, enhance patient compliance, and increase bioavailability due to its absence of hepatic first-pass metabolism.[16,17] However, the skin's barrier function represents a significant challenge to drug penetration,[18,19] particularly regarding the stratum corneum (SC).[20] To overcome this challenge, researchers have explored a range of strategies to promote transdermal drug absorption and penetration. These approaches include microneedles (MNs),[21] iontophoresis,[22,23] sonophoresis,[24] magnetophoretic,[25] electroporation,[26,27] and photomechanical waves.[28] Nevertheless, conventional methods such as electric methods-iontophoresis and electroporation, and magnetophoretic can create nanosized pores to improve the permeability.[29] For insoluble drugs, ionic liquids, sonophoresis, and other technologies cannot substantially break through the SC barrier,[30,31] which greatly affects the permeation efficiency of drugs. In addition, these methods employ sophisticated equipment and complex preparation processes, which may result in discomfort comparable to that experienced during standard needle injection. MNs are an array of micron-sized needles. They represent the most viable method for circumventing the SC barrier to deliver therapeutic drugs to the skin.[32,33] Additionally, the length of the MN is only 0.2 to 1.5 mm, which allows for painless penetration of the skin's SC while maintaining minimal invasiveness.[34–37]

The drug transport method classifies MN patches into five types: solid MNs,[38] hollow MNs,[39] coated MNs,[40] dissolving MNs,[41] and hydrogel-forming MNs.[42] The first three types of MNs are manufactured from silicon or metals, and if the needle breaks during administration, it can cause significant damage to the skin.[43] The safety of emerging materials such as poly (methyl vinyl ether) co-maleic acid (PMVE/MA) and methacrylate hyaluronic acid for the preparation of hydrogel MNs has yet to be confirmed.[44] However, the composition of dissolving MNs includes water-soluble matrix materials such as polylactic acid, polyvinyl pyrrolidone (PVP), hyaluronic acid, polyvinyl alcohol, and chitosan. The drug is dispersed or dissolved in the needle.[45–49] After insertion into the skin, the needle dissolves when it absorbs water from the interstitial fluid and releases the drug payload. As a result, the drug is delivered directly to the skin for therapeutic effect without leaving a sharp needle.[50–52] Additionally, when they come into contact with moisture in the dermis, the tip dissolves rapidly, thereby facilitating the recovery of damaged skin and minimizing the risk of infection.[53] Currently, dissolving MNs have been developed to deliver a range of drugs, including genes, peptides, vaccines, and proteins.[54–57]

In this study, a two-step casting procedure was employed to prepare dissolving MNs for loading Res in the needle tips, for the first time. PVP K90 was selected as the matrix material. The mechanical properties, morphology, and skin permeability of the MNs were characterized. Furthermore, the puncture performance, skin recovery, and drug release profiles following MN treatment were evaluated.

Materials and Methods

Materials

Res (purity $>$ 99%) was purchased from Shanghai Aladdin Biochemical Technology Co., Ltd. (Shanghai, China). PVP K90 (Mw = 395.2 Da) was purchased from Boai New Open Source Medical Technology Group Co., Ltd. (Jiaozuo, China). Glycerin was obtained from Xilong Science Co., Ltd. (Shantou, China). Sodium carboxymethyl cellulose was purchased from Anhui Shanhe Medicinal Accessories Co., Ltd. (Anhui, China). Methanol was purchased from Thermal Fisher Technology Co., Ltd. (Massachusetts, United States). Anhydrous ethyl alcohol was purchased from National Pharmaceutical Group Chemical Reagent Co., Ltd. (Shanghai, China). Chloral hydrate and Laurocapram were purchased from Shanghai MacLean Biochemical Technology Co., Ltd. (Shanghai, China). Phosphate-buffered saline (PBS) was purchased from Wuhan Punosai Biotechnology Co., Ltd. (Wuhan, China). Methylene blue was purchased from Sigma-Aldrich Shanghai Trading Co., Ltd. (Shanghai, China). All other reagents were of analytical grade and purified water was used throughout this study.

Male Sprague Dawley (SD) rats (200 $\pm$ 20 g) were provided by the Experimental Animal Center of Jiangxi University of Chinese Medicine (Nanchang, China).

Fabrication of Res-Loaded Microneedles

Dissolving MNs were prepared by the two-step casting method.[58] PVP K90 was selected as the best matrix material for the preparation of MN tips through our pretesting. Briefly, the mixture of tip material and drug was poured into the MN mold (Taizhou, China). After centrifugation at 5,000 r/min for 10 minutes, and removing the excess needle tip solution, the MN mold was kept in a desiccator, dying at room temperature for 30 minutes. Subsequently, the backing material was poured into the MN mold and centrifuged at 3,000 r/min for 5 minutes. The mold is placed in a desiccator and dried at 30°C for 24 hours. Finally, the dissolving MNs were demolded and placed in a desiccator before the experiment.

The tip materials were prepared as follows. The tip solution was prepared by dissolving PVP K90 in a certain amount of methanol-aqueous solution for ultrasonic dissolution, then Res powder was added to acquire a mixture of a polymer blend.

The backing materials were prepared as follows. PVP K90 (12 g) and glycerol (0.45 g) were placed in ultra-pure water (30 mL), stirred until completely dissolved, removed bubbles by ultrasound, and set aside before the experiment.

Optimization of Res-Loaded Microneedles

Box–Behnken design, a response surface methodology,[59] was employed, with centrifugation time (A), solvent concentration (B), and prescription ratio (Res: matrix) (C) as the investigated index. Two levels of each independent variable were employed. The parameter values of the independent variable (A, B, and C) were based on the results of previous single-factor experiments (data were not shown), and Res drug loading (Y) was selected as the dependent variable. The parameters and values are detailed in ►**Table 1**. Design-

Table 1 Selected independent and dependent variable levels

	Level	
Independent variables	Lower limit (−1)	Higher limit (+1)
A	5	15
B	20	30
C	0.3	0.5
Dependent variable	Constraints	
Y	Maximize	

Abbreviations: A, centrifugation time (min); B, solvent concentration (%); C, prescription ratio (Res: matrix); Y, drug loading of Res-MNs (μg).

Expert software (Stat-Ease, Wilmington, United States) was used to optimize the correlation between the independent and dependent variables by generating mathematical equations, contour, and response surface designs. Accordingly, the experiment was divided into 17 batches. The criteria for selecting of optimum formulation were mainly based on the maximum drug loading.

Characterizations of Microneedles

The geometry of Res-MNs was evaluated by scanning electron microscope to characterize the size of the MNs, the tip morphology, and the distribution of the MNs on the array.

Mechanical Strength of Microneedles

The aluminum foil was laid flat, the tip of the Res-loaded MN was placed downward, and the MN was pressed by applying a force of about 10 N with the thumb for about 30 seconds.[60] The MN punctured the aluminum foil. The porosity of the MN and the morphology of the MN after puncture were assessed.

Methylene blue MNs were prepared by a two-step centrifugation method of methylene blue solution (1 mg/mL, 2 mL) and PVP K90 (300 mg). Eight-week-old male SD rats were anesthetized with 5% chloral hydrate solution, and the abdominal hair was removed with depilatory cream and wiped clean. Subsequently, the methylene blue MNs were pressed on the rat's abdominal skin and maintained for 10 seconds. After 2 minutes, the MNs were removed. The punctured skin was observed under an optical microscope.

Solubility of Microneedles after Insertion

The dissolution of MN after skin puncture was observed. Male SD rats were anesthetized with 5% chloral hydrate and their abdominal hair was removed with a depilatory cream. The MNs were pressed on the abdominal skin of the rats with a force of about 10 N/cm^2. The MNs were removed from the skin at predetermined intervals of 1, 5, 10, and 20 minutes, respectively. The dissolved morphology of MNs was observed under an optical microscope.

Safety Evaluation of Res-Microneedles

To prevent the entry of pathogenic microorganisms and toxic substances, and to reduce the risk of infection, microchannels created by MNs need to be quickly closed after administration. The MNs were inserted into the depilated skin and fixed with medical tape. Five minutes later, the MNs were removed from the skin. The micropores in the skin were photographed with a digital camera at 0, 1, 2, 3, 6, and 12 hours, respectively, until the micropore in the skin became invisible.

Saturation Solubility Test

The solubilization of PVP K90 for Res was evaluated. Briefly, PVP K90 (25, 50, and 100 mg) was dissolved in aqueous solution (1 mL), respectively, ultrasonic dissolution for 15 minutes, cooled and added to Res (5 mg) to achieve a mixture containing: (1) Res: PVP K90 (1:5, w/w), (2) Res: PVP K90 (1:10, w/w), and (3) Res: PVP K90 (1:20, w/w). The Eppendorf tubes containing solvents and drugs were agitated on a thermostatically controlled orbital shaker at 37 ± 2°C at a speed of 200 r/min for 24 hours. The sample was centrifugated to settle down. The supernatant solution was filtered through a 0.22-μm filter and analyzed by high-performance liquid chromatography (HPLC) method. The blank group only added the same amount of Res (Res aqueous solution).

Skin Permeability of Res-Loaded Microneedles

The skin permeability of Res-loaded MN was assessed using a multifunction transdermal diffuser (TP-6, Tianjin, China) and a horizontal diffusion cell (TP-6, Tianjin, China). The diffusion cell contains a donor chamber and an acceptor chamber, with male SD rat's skin (2 cm × 2 cm) being located between the chambers. The underside layer was in contact with the acceptor chamber fluid. The acceptor chamber was filled with the dissolution medium (PBS, pH = 7.4) and stirred at 600 rpm, maintaining the temperature at 37°C.

Res (30 mg) and purified water (10 mL) were mixed to form Res suspension (Res-SUS, 3 mg/mL). Res (30 mg) and sodium carboxymethyl cellulose (0.5 g) were dissolved in purified water (10 mL), and then laurazone (0.1 mL) was added to form Res gel solution (Res-GEL, 3 mg/mL).

The skin was treated with Res-MNs, Res-SUS, and Res-GEL, respectively, and then sandwiched between the chambers. Res-MNs were applied to the surface of the skin and pressed continuously for 1 minute with a force of about 10 N. Res-SUS (0.1 mL) and Res-GEL (0.1 mL) were applied on the skin of rats. At intervals of 1, 2, 3, 4, 6, 8, 12, and 24 hours, respectively, a sample (an aliquot of 0.2 mL) was collected from the sampling port of the acceptor chamber, and an equal volume of dissolved medium was added to maintain the sink condition. The content of Res in the samples was analyzed by the HPLC method.

High-Performance Liquid Chromatography Analysis

The content of Res in the MNs was determined. Briefly, the tips of the MN patch were removed from the bottom with a scalpel and dissolved in 2 mL methanol solution. The solution was swirled for 5 minutes, followed by centrifuging at 4,000 rpm for 10 minutes. The supernatant was collected and diluted properly, and Res content in the solution was determined by an LC-20A HPLC (Shimadzu, Kyoto, Japan)

with a diamond C18 column (4.6 mm × 250 mm, 5 µm, California, United States). The flow rate was 1 mL/min and the column temperature was 30°C. The mobile phase consisted of an equal volume of methanol and water. The detection wavelength was 308 nm and the injection volume was 20 µL. In the range of 0.1 to 50 µg/mL, there was a good linear relationship between the peak area (A) and the concentration of Res (X). The regression equation was $A = 136{,}382X + 1{,}271.2$ ($R^2 = 0.9998$). The extraction recovery rate, accuracy, and precision all meet the requirements of biological sample analysis.

Data Analysis

All data were presented as mean ± standard deviation. All experiments were repeated at least three times. SPSS Statistics 22.0 (SPSS Inc., Chicago, Illinois, United States) with one-way analysis of variance was used for statistical analysis. A p-value of less than 0.05 is considered statistically significant.

Results and Discussion

Formulation Optimization of Microneedles

With the drug loading of MNs as an index, test results of (A) centrifugation time, (B) solvent concentration, and (C) formulation are shown in ►**Table 2**. Analysis was conducted using Design Expert 8.0.6 software, and the regression equation of the drug loading of MNs was obtained as follows: $Y = 85.84 + 0.7085A + 0.6292B + 0.1900C - 0.0675AB - 0.6621AC - 0.1161BC - 1.78A^2 - 1.70B^2 - 1.13C^2$.

The model was established, and then a multiple quadratic regression response surface model of MN drug loading was obtained. The test results of the influencing factors (A, B, and C) were analyzed by multiple linear regression and binomial fitting analysis to verify the significance of the regression model and influencing factors. As can be seen from ►**Table 3**, $F = 7.01$ and $p = 0.0088$ in the established regression model. It shows that the difference in the regression model is very significant. The p-value of the lack of fitting term is 0.55, which is above 0.05, and as a result, the difference in the model is not significant, indicating that the equation is reliable. Our data indicated that the test design is reliable, accords with the actual situation, and is realistic enough to be used in the analysis. Therefore, it is feasible to use this model to analyze and predict the drug loading of MNs.

From the p-value in ►**Table 3**, it can be seen that the centrifugation time (A) in the primary item has a significant effect on the drug loading of MNs. In the quadratic term, the effect of secondary terms A^2 and B^2 have extremely significant effects on the drug loading of MNs, and C^2 has significant effects on the drug loading of MNs. In the interaction terms, AB, AC, and BC had no significant effect on the drug loading of MNs. According to the F value in ►**Table 3**, it can be concluded that the effects of three factors on MN drug loading are centrifugation time (A) > solvent concentration (B) > prescription ratio (C).

►**Fig. 1** was the response surface and contour map of interaction effects of preparation conditions (A, B, and C) created by the response surface regression model. The

Table 2 Independent values and response for formulations in Box–Behnken design

Formulations	Independent variables			Response Y (µg)
	A (min)	B (%)	C	
1	15	20	0.375	82.56
2	10	25	0.375	86.93
3	5	20	0.375	81.22
4	5	25	0.500	82.64
5	10	25	0.375	85.01
6	15	30	0.375	83.11
7	10	25	0.375	85.77
8	10	25	0.375	86.12
9	10	30	0.300	83.73
10	10	20	0.300	81.45
11	10	20	0.500	82.67
12	15	25	0.500	83.14
13	10	25	0.375	84.78
14	5	30	0.375	82.04
15	5	25	0.300	81.25
16	15	25	0.300	84.67
17	10	30	0.500	84.17

Abbreviations: A, centrifugation time (min); B, solvent concentration (%); C, prescription ratio (Res: matrix); Y, drug loading of Res-MNs (µg).

Table 3 Analysis of variance of regression model

Source	Sum of squares	Freedom	Mean square	*F*-value	*p*-Value	Significant
Model	43.73	9	4.86	7.0100	0.0088	[b]
A-Centrifugation time (min)	3.90	1	3.90	5.6300	0.0495	[a]
B-Solvent concentration (%)	3.07	1	3.07	4.4400	0.0732	
C-Prescription ratio (Res: matrix)	0.2888	1	0.2888	0.4168	0.5391	
AB	0.0182	1	0.0182	0.0263	0.8757	
AC	1.81	1	1.81	2.6100	0.1502	
BC	0.0556	1	0.0556	0.0802	0.7852	
A^2	13.41	1	13.41	19.360	0.0032	[b]
B^2	12.24	1	12.24	17.660	0.0040	[b]
C^2	4.58	1	4.58	6.6100	0.0370	[a]
Residual	4.85	7	0.6929			
Lack of fit	1.84	3	0.6119	0.8120	0.5500	
Pure error	3.01	4	0.7536			
Total difference	48.58	16				

Note: The data are presented as the mean ± standard deviation.
[a]$p < 0.05$.
[b]$p < 0.01$.

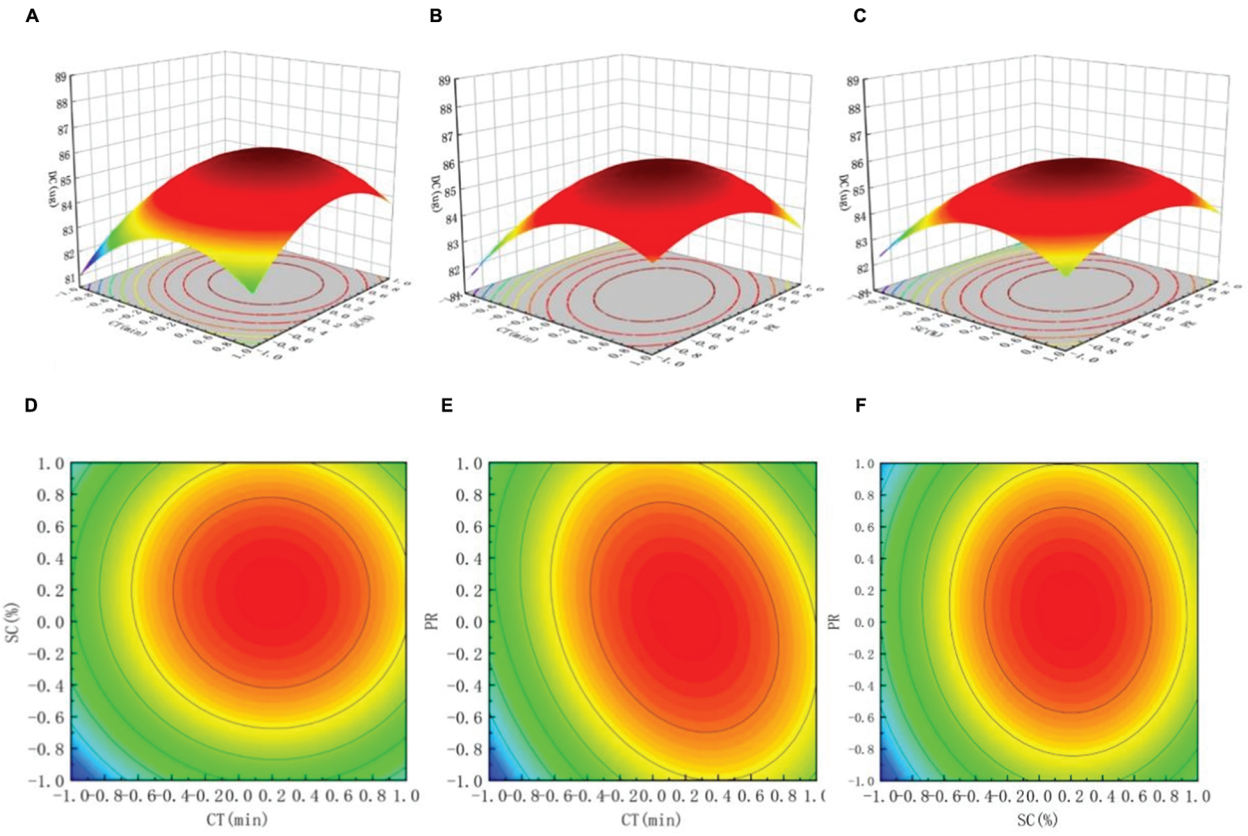

Fig. 1 3D response surface plots (**A**, **B**, and **C**) and 2D contour maps (**D**, **E**, and **F**) for the impact of independent variables on drug loading. (**A**) Centrifugation time versus solvent concentration. (**B**) Centrifugation time versus prescription ratio. (**C**) Prescription ratio versus solvent concentration. (**D**) 2D contour maps of centrifugation time versus solvent concentration. (**E**) 2D contour maps of centrifugation time versus prescription ratio. (**F**) 2D contour maps of prescription ratio versus solvent concentration. 2D, two-dimensional; 3D, three-dimensional.

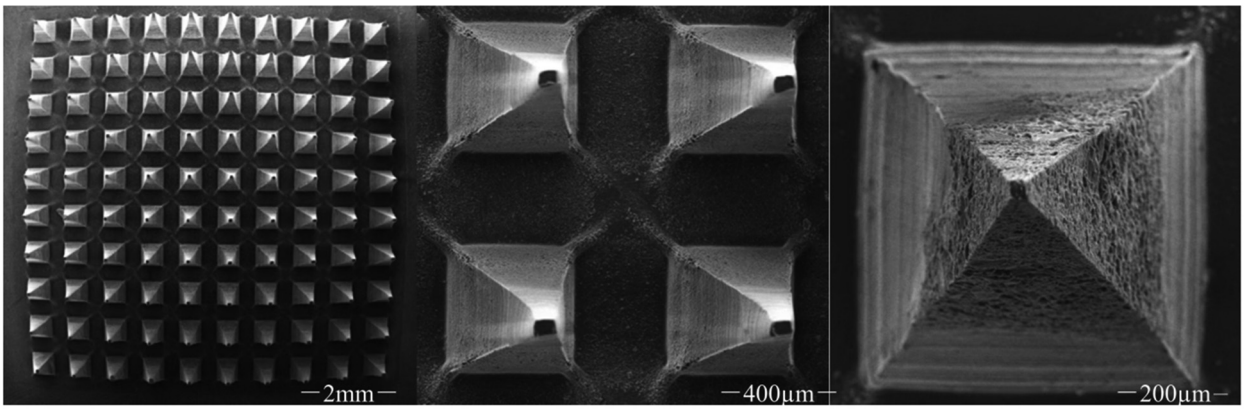

Fig. 2 Representative SEM images of dissolving MNs. MNs, microneedles; SEM, scanning electron microscope.

regression fitting equation of MN drug loading was solved, and the best preparation conditions were obtained: A = 10.95, B = 25.90, C = 0.40. Under this condition, the drug loading of MNs was 85.96 μg. According to the feasibility of the experiment and practical operation, the conditions for preparing dissolving MNs were as follows: centrifugation time was 10 minutes, solvent concentration was 25%, and prescription ratio was 0.375. Under these conditions, the drug loading of MNs was 85.72 μg. The relative error of the predicted value of the model was only 0.24 μg, indicating that the drug loading conditions of MNs were optimized by the response surface method, and the parameters of the preparation scheme were accurate and reliable and had a certain application value.

Although our optimized MN drug loading only varies between 80 and 87 μg (►**Table 2**), a small increase in drug loading is also meaningful. For insoluble drugs, it can increase the exposure of drugs to increase the bioavailability. For MN drug delivery, the dose given is only equivalent to that of the traditional dosage form 1/5 to 1/200,[61,62] which can effectively reduce the number of MN patches. According to existing research, the effective dose of Res in regulating Human Bone marrow mesenchymal stem cells is 0.1 to 1 μmol/L to regulate self-renewal and multipotency through the SIRT1-SOX2 axis.[63] In this paper, the drug loading of each MN was about 86 μg, which is sufficient to exert the curative effect of Res.

Characterizations

PVP K90 was a nonionic amorphous polymer, which was widely used in transdermal drug delivery systems because of its solubility in water. In addition, PVP K90 did not cause skin irritation or sensitization.[64,65] Therefore, PVP-K90 was used to modulate the mechanical strength and brittleness of MNs. As shown in ►**Fig. 2**, Res-MNs had a complete needle shape, which was quadrangular pyramid-shaped, and the MN plaque was square, the needles were arranged in a 10×10 array in a patch of $8\,mm \times 8\,mm$. Compared with pyramids and circles, this shape had better penetration and higher skin delivery efficiency. The height of MN was $762.5 \pm 1.56\,\mu m$, and the distance between MN was $295 \pm 1.25\,\mu m$. The length of the MN mold was 800 μm and the MN spacing was 300 μm. Compared with the mold, the size of the prepared MN shrinks slightly, which may be due to the rapid volatilization of the solvent during the drying process. When preparing Res-MNs, we choose 25% methanol solution as a solvent, which not only can effectively inhibit the diffusion of drugs in the tip to the backing layer but also reduces the large number of bubbles caused by solvent volatilization in the preparation of MN patches.[66] As a result, the influence on the mechanical strength and drug loading of MNs can be effectively reduced.

Mechanical Strength

As shown in ►**Fig. 3A**, **B**, Res-MN effectively pierced the aluminum foil and formed 100 holes, and the puncture efficiency (PE) was 100%. As shown in ►**Fig. 3C**, MN pinholes are dotted on rat skin, consistent with the MN array, with a PE of 100%, indicating that the MNs have sufficient mechanical strength to puncture the skin and overcome the SC.

Microneedle Dissolution *in vivo*

The abdominal skin of SD rats was used to evaluate the dissolution of MNs *in vivo*. The morphological changes of MNs after insertion into 1, 5, 10, and 20 minutes were observed by optical microscopy, respectively. As shown in ►**Fig. 4**, the tip of the MN dissolved in the skin after 1 minute, and the MN gradually dissolved over time. After 20 minutes, MNs completely dissolved in the skin. The above results show that MNs could dissolve in the skin and release drugs into the skin after contact with active epidermis or dermis tissue fluid within a few minutes. The rapid dissolution of MNs helps to be reliable and easy to use in practice, making patients more compliant.

Application Safety of Res-Microneedles

The recovery of skin after MN treatment was observed by a digital camera. As shown in ►**Fig. 5**, the micropores formed by MNs almost disappeared 3 hours after implantation, and only slight wounds were left in the skin. The puncture marks gradually disappeared over time, and the spots on the skin wounds vanished completely within 12 hours later. No obvious irritant reaction was observed during the observation period. To sum up, MNs could penetrate the SC and transport Res directly to the skin lesions, resulting in minor and

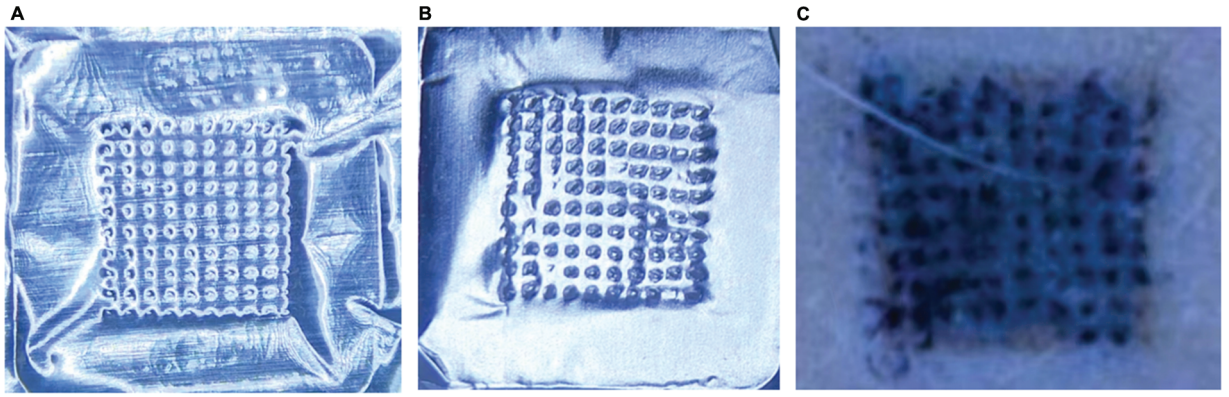

Fig. 3 Insertion capacity of the MNs. (**A**) Conventional frontal aluminum foil shooting image. (**B**) Conventional back aluminum foil shooting image. (**C**) Staining image of skin puncture with methylene blue MNs. MNs, microneedles.

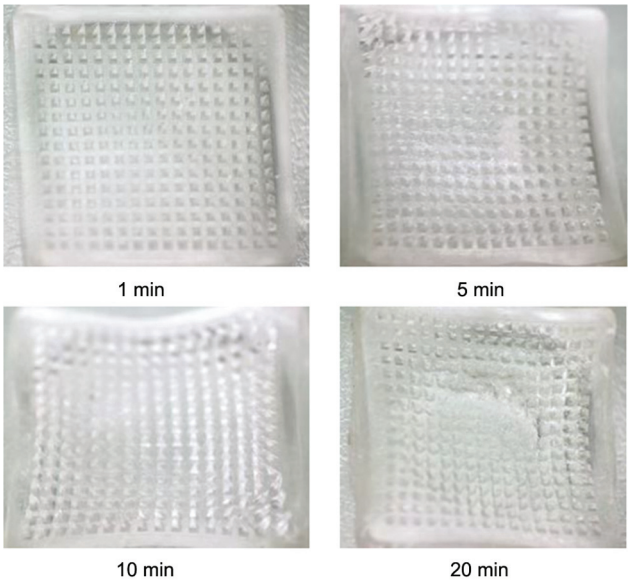

Fig. 4 Morphological changes of MNs dissolution after insertion into the abdominal skin of SD rats at 1, 5, 10, and 20 minutes. MNs, microneedles; SD, Sprague Dawley.

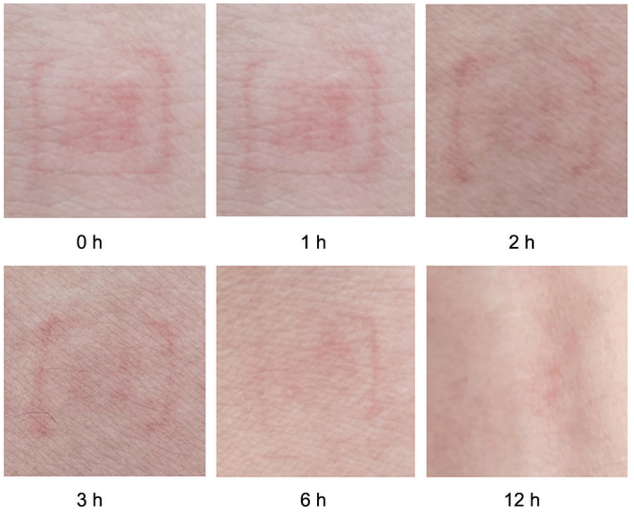

Fig. 5 The skin recovery within 12 hours after administration of Res-MNs. Res-MNs, resveratrol-loaded dissolving microneedles.

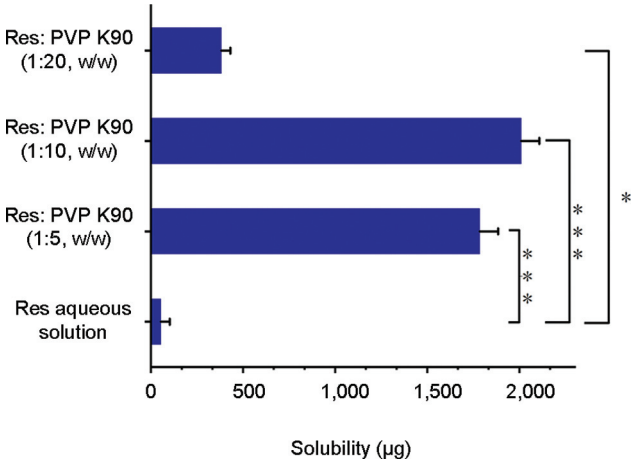

Fig. 6 The solubilization effect of PVP K90 on Res detected by HPLC. Data were represented as mean ± standard deviation ($n = 3$; $^{*}p < 0.05$; $^{***}p < 0.001$ versus Res aqueous solution). HPLC, high-performance liquid chromatography; Res, resveratrol.

reversible damage, which greatly increases the convenience and acceptability of frequent administration.

Saturation Solubility of Res

The solubility of drugs and matrix materials in solvents was very important to determine whether the drug distribution in the MNs was uniform and whether the drug loading was sufficient. PVP K90 was selected as the matrix material of MNs, not only for its good biocompatibility but also for its good water solubility.[67] As shown in ►**Fig. 6**, the saturated solubility of Res in different proportions of PVP K90 solution was 1,783.9 ± 10.45 μg/mL (Res: PVP K90, 1:5), 2,008.2 ± 12.5 μg/mL (Res: PVP K90, 1:10), and 380.4 ± 7.44 μg/mL (Res: PVP K90, 1:20), respectively. However, the average solubility of Res in ultra-pure water was only 51.9 ± 5.4 μg/mL. The Res solubility of Res: PVP K90 (1:5, w/w) and Res: PVP K90 (1:10, w/w) was 34 and 38 times higher than that of Res aqueous solution, respectively, and the difference was extremely significant ($p < 0.001$). The Res solubility of Res: PVP K90 (1:20, w/w) was about 7 times higher than that of Res aqueous solution, but there was also a significant ($p < 0.05$). It's worth exploring whether the Res

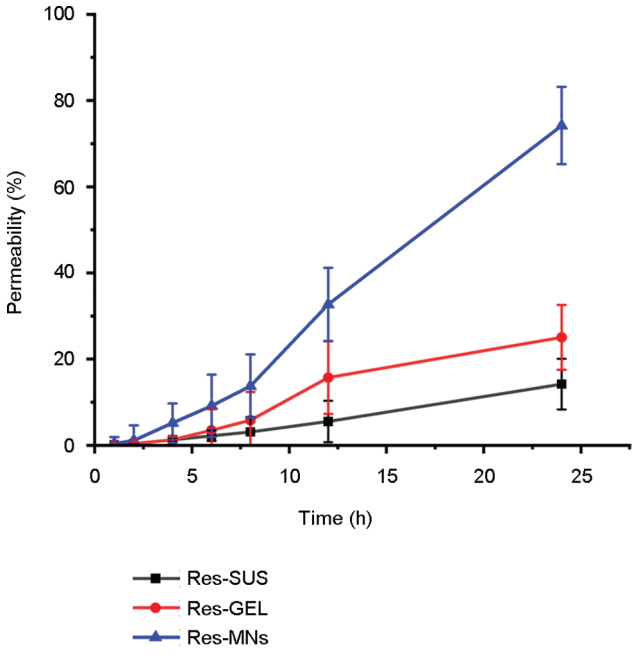

Fig. 7 *In vitro* penetration curves of Res-MNs, Res-SUS, and Res-GEL. Data were presented as mean ± standard deviation ($n = 3$). Res-MNs, resveratrol-loaded dissolving microneedles; Res-SUS, resveratrol suspension; Res-GEL, resveratrol gel solution.

solubility of Res: PVP K90 (1:20, w/w) was lower than Res: PVP K90 (1:5, w/w) and Res: PVP K90 (1:10, w/w). The result of higher the concentration of PVP K90 in the solution, the greater its viscosity, thus affecting the infiltration of water in the solution into Res and reducing its solubilization. For the other two groups, the low concentration of PVP K90 has lower viscosity, the main effect on Res is to increase the dispersion in the solution. Therefore, not only did the specific surface area of Res improve, but also the hydrophilicity.[68]

In vitro Skin Penetration of Res-Microneedles

Many previous studies have confirmed that dissolving MNs could be used as an effective tool to improve the permeability and delivery efficiency of drugs.[69] In this experiment, the abdominal skin of SD rats was used as a drug-permeable membrane. The permeation profiles of Res from different approaches are shown in ►**Fig. 7**. The Res-MN was the highest among all groups at all time points. Pretreatment with solid MNs created micropores in the skin, facilitating the diffusion of the Res from the skin SC into the skin dermis. The results showed that the Res-MN released about 35% of the drug within 12 hours, and then slowly released the drug over time. Finally, about 75% of the drug was released within 24 hours. The Res-SUS and the Res-GEL had a lower speed of drug delivery, and about 13 and 25% of the drugs were delivered within 12 hours, respectively. Res-MN had excellent drug delivery efficiency, with 5 and 3 times that of the Res-SUS and the Res-GEL within 24 hours. The results confirmed the promoted effect of MN on the penetration of Res into the skin due to the micropores created by the MN patch.[70] Furthermore, Res content delivered to the receiver compartment was less than that in the needle, presumably because of the residual drug in the skin.[71]

Conclusion

In the present work, we developed a dissolvable polymeric MN patch loaded with Res to enhance the absorption of Res in transdermal administration. The Res-MNs were optimized through the application of the Box–Behnken experimental design method. The MNs, prepared from the matrix of PVP-K90, exhibited a smooth body, a sharp tip, and no obvious pores or gaps on the surface. It demonstrated good mechanical strength, enabling penetration of the skin. Moreover, the obtained MN dissolved rapidly upon absorption of interstitial fluid following insertion. In addition, the pinhole created by the MN can be expected to heal within 12 hours, indicating excellent skin recovery. Most notably, the PVP K90 demonstrated a pronounced solubilization effect on Res, markedly enhancing the drug-loading capacity of Res within MNs. *In vitro*, transdermal release studies demonstrated that Res-MNs exhibited excellent drug delivery efficiency, with a drug delivery amount of about 5 and 3 times that of the Res-SUS and the Res-GEL, respectively, within 24 hours. To sum up, Res-MNs manufactured from PVP-K90 not only enhance the solubility of Res but also exhibit notable advantages in transdermal delivery. Nevertheless, further animal studies are required to assess the pharmacokinetic and pharmacodynamic profiles of the Res-MNs for their potential clinical application.

Ethical Approval

This work was approved by the Animal Ethics Committee and abides by the relevant agreements of the National Pharmaceutical Engineering Center for Solid Preparation in Chinese Herbal Medicine, Jiangxi University of Traditional Chinese Medicine.

Funding

This research was funded by the Natural Science Foundation of Jiangxi Province (Grant No. 20242BAB23090), the Jiangxi University of Chinese Medicine Science and Technology Innovation Team Development Program (Grant Nos. CXTD-22008, CXTD-22004), the PhD startup foundation of Affiliated Hospital of Jiangxi University of Chinese Medicine (Grant No. 23KYQDZJ02) and the students' innovation and entrepreneurship training program (Grant Nos. 202110412009, 202210412312).

Conflict of Interest

None declared.

References

1 Ren J, Liu H, Hao Y, He P, Fang Y. Determination of resveratrol in red wine by solid phase extraction-flow injection chemiluminescence method. Chin Chem Lett 2007;18:985–988
2 Zhang Q, Bian Y, Shi Y, et al. An economical and efficient technology for the extraction of resveratrol from peanut (Arachis hypogaea) sprouts by multi-stage countercurrent extraction. Food Chem 2015; 179:15–25

3 Ros E, Singh A, O'Keefe JH. Nuts: natural pleiotropic nutraceuticals. Nutrients 2021;13(09):3269
4 Abdel Bar FM, Abbas GM, Gohar AA, Lahloub MI. Antiproliferative activity of stilbene derivatives and other constituents from the stem bark of *Morus nigra* L. Nat Prod Res 2020;34(24):3506–3513
5 Ungurianu A, Zanfirescu A, Margină D Sirtuins, resveratrol and the intertwining cellular pathways connecting them. Ageing Res Rev 2023;88:101936
6 Chedea VS, Vicaş SI, Sticozzi C, et al. Resveratrol: from diet to topical usage. Food Funct 2017;8(11):3879–3892
7 Cho S, Namkoong K, Shin M, et al. Cardiovascular protective effects and clinical applications of resveratrol. J Med Food 2017;20(04):323–334
8 Ko JH, Sethi G, Um JY, et al. The role of resveratrol in cancer therapy. Int J Mol Sci 2017;18(12):2589
9 Kotecha R, Takami A, Espinoza JL. Dietary phytochemicals and cancer chemoprevention: a review of the clinical evidence. Oncotarget 2016;7(32):52517–52529
10 Nawaz W, Zhou Z, Deng S, et al. Therapeutic versatility of resveratrol derivatives. Nutrients 2017;9(11):1188
11 Tang H, Xiang S, Li X, Zhou J, Kuang C. Preparation and *in vitro* performance evaluation of resveratrol for oral self-microemulsion. PLoS One 2019;14(04):e0214544
12 Annaji M, Poudel I, Boddu SHS, Arnold RD, Tiwari AK, Babu RJ. Resveratrol-loaded nanomedicines for cancer applications. Cancer Rep (Hoboken) 2021;4(03):e1353
13 Tosato MG, Maya Girón JV, Martin AA, Krishna Tippavajhala V, Fernández Lorenzo de Mele M, Dicelio L. Comparative study of transdermal drug delivery systems of resveratrol: high efficiency of deformable liposomes. Mater Sci Eng C 2018;90:356–364
14 Sinha D, Sarkar N, Biswas J, Bishayee A. Resveratrol for breast cancer prevention and therapy: preclinical evidence and molecular mechanisms. Semin Cancer Biol 2016;40-41:209–232
15 Pujara N, Jambhrunkar S, Wong KY, McGuckin M, Popat A. Enhanced colloidal stability, solubility and rapid dissolution of resveratrol by nanocomplexation with soy protein isolate. J Colloid Interface Sci 2017;488:303–308
16 Qu F, Geng R, Liu Y, Zhu J. Advanced nanocarrier- and microneedle-based transdermal drug delivery strategies for skin diseases treatment. Theranostics 2022;12(07):3372–3406
17 Zhang Y, Liu C, Wang JQ, et al. Ionic liquids in transdermal drug delivery system: current applications and future perspectives. Chin Chem Lett 2023;34:107631
18 Alany R. Topical and transdermal formulation and drug delivery. Pharm Dev Technol 2017;22(04):457
19 Prausnitz MR, Langer R. Transdermal drug delivery. Nat Biotechnol 2008;26(11):1261–1268
20 Dharadhar S, Majumdar A, Dhoble S, Patravale V. Microneedles for transdermal drug delivery: a systematic review. Drug Dev Ind Pharm 2019;45(02):188–201
21 Zhang X, Wang Y, Chi J, Zhao Y. Smart microneedles for therapy and diagnosis. Research (Wash D C) 2020;2020:7462915
22 Zuo J, Du L, Li M, Liu B, Zhu W, Jin Y. Transdermal enhancement effect and mechanism of iontophoresis for non-steroidal anti-inflammatory drugs. Int J Pharm 2014;466(1-2):76–82
23 Andrade JFM, Cunha-Filho M, Gelfuso GM, Gratieri T. Iontophoresis for the cutaneous delivery of nanoentraped drugs. Expert Opin Drug Deliv 2023;20(06):785–798
24 Seah BC, Teo BM. Recent advances in ultrasound-based transdermal drug delivery. Int J Nanomedicine 2018;13:7749–7763
25 Sammeta SM, Repka MA, Narasimha Murthy S. Magnetophoresis in combination with chemical enhancers for transdermal drug delivery. Drug Dev Ind Pharm 2011;37(09):1076–1082
26 Huang D, Huang Y, Li Z. Transdermal delivery of nucleic acid-mediated by punching and electroporation. Methods Mol Biol 2020;2050:101–112
27 Zhang H, Jin WR. Determination of amino acids in an individual erythrocyteby capillary electrophoresis with intracellular FITC-derivatization and laser-induced fluorescence detection. Chin Chem Lett 2003;14:952–954
28 Dradrach K, Rogóż M, Grabowski P, et al. Traveling wave rotary micromotor based on a photomechanical response in liquid crystal polymer networks. ACS Appl Mater Interfaces 2020;12 (07):8681–8686
29 Sharma D. Microneedles: an approach in transdermal drug delivery: a review. Pharmatutor 2018;6:07
30 Ali MK, Moshikur RM, Goto M, Moniruzzaman M. Recent developments in ionic liquid-assisted topical and transdermal drug delivery. Pharm Res 2022;39(10):2335–2351
31 Park D, Won J, Lee G, Lee Y, Kim CW, Seo J. Sonophoresis with ultrasound-responsive liquid-core nuclei for transdermal drug delivery. Skin Res Technol 2022;28(02):291–298
32 Chen Z, Lv Y, Qi J, Zhu Q, Lu Y, Wu W. Overcoming or circumventing the stratum corneum barrier for efficient transcutaneous immunization. Drug Discov Today 2018;23(01):181–186
33 Pireddu R, Schlich M, Marceddu S, et al. Nanosuspensions and microneedles roller as a combined approach to enhance diclofenac topical bioavailability. Pharmaceutics 2020;12(12):1140
34 Sheng T, Luo B, Zhang W, et al. Microneedle-mediated vaccination: innovation and translation. Adv Drug Deliv Rev 2021; 179:113919
35 Ramaut L, Hoeksema H, Pirayesh A, Stillaert F, Monstrey S. Microneedling: where do we stand now? A systematic review of the literature. J Plast Reconstr Aesthet Surg 2018;71(01): 1–14
36 Kapoor Y, Milewski M, Dick L, et al. Coated microneedles for transdermal delivery of a potent pharmaceutical peptide. Biomed Microdevices 2019;22(01):7
37 Chen Z, He J, Qi J, Zhu Q, Wu W, Lu Y. Long-acting microneedles: a progress report of the state-of-the-art techniques. Drug Discov Today 2020;25(08):1462–1468
38 Tan JY, Li Y, Chamani F, et al. Experimental validation of diffraction lithography for fabrication of solid microneedles. Materials (Basel) 2022;15(24):8934
39 Cárcamo-Martínez Á, Mallon B, Domínguez-Robles J, Vora LK, Anjani QK, Donnelly RF. Hollow microneedles: a perspective in biomedical applications. Int J Pharm 2021;599:120455
40 Matadh AV, Jakka D, Pragathi SG, et al. Polymer-coated polymeric (PCP) microneedles for controlled dermal delivery of 5-fluorouracil. AAPS PharmSciTech 2022;24(01):9
41 Sartawi Z, Blackshields C, Faisal W. Dissolving microneedles: applications and growing therapeutic potential. J Control Release 2022;348:186–205
42 Liu Y, Huang T, Qian ZY, Chen W. Extensible and swellable hydrogel-forming microneedles for deep point-of-care sampling and drug deployment. Chin Chem Lett 2023;34:108103
43 Ita K. Dissolving microneedles for transdermal drug delivery: advances and challenges. Biomed Pharmacother 2017; 93:1116–1127
44 Sullivan SP, Koutsonanos DG, Del Pilar Martin M, et al. Dissolving polymer microneedle patches for influenza vaccination. Nat Med 2010;16(08):915–920
45 Ronnander P, Simon L, Koch A. Experimental and mathematical study of the transdermal delivery of sumatriptan succinate from polyvinylpyrrolidone-based microneedles. Eur J Pharm Biopharm 2020;146:32–40
46 Song YY, Dong CM. Sugar-dependent targeting and immune adjuvant effects of hyperbranched glycosylated polypeptide nanoparticles for ovalbumin delivery. Chin Chem Lett 2022; 33:4084–4088
47 Nguyen HX, Bozorg BD, Kim Y, et al. Poly (vinyl alcohol) microneedles: fabrication, characterization, and application for transdermal drug delivery of doxorubicin. Eur J Pharm Biopharm 2018; 129:88–103
48 Wu L, Shrestha P, Iapichino M, Cai Y, Kim B, Stoeber B. Characterization method for calculating diffusion coefficient of drug from

polylactic acid (PLA) microneedles into the skin. J Drug Deliv Transl 2021;61:102192
49 He J, Zhang Z, Zheng X, et al. Design and evaluation of dissolving microneedles for enhanced dermal delivery of propranolol hydrochloride. Pharmaceutics 2021;13(04):579
50 Maurya A, Nanjappa SH, Honnavar S, Salwa M, Murthy SN. Rapidly dissolving microneedle patches for transdermal iron replenishment therapy. J Pharm Sci 2018;107(06):1642–1647
51 Pei P, Yang F, Liu J, et al. Composite-dissolving microneedle patches for chemotherapy and photothermal therapy in superficial tumor treatment. Biomater Sci 2018;6(06):1414–1423
52 Ahmed Saeed Al-Japairai K, Mahmood S, Hamed Almurisi S, et al. Current trends in polymer microneedle for transdermal drug delivery. Int J Pharm 2020;587:119673
53 Hong X, Wei L, Wu F, et al. Dissolving and biodegradable microneedle technologies for transdermal sustained delivery of drug and vaccine. Drug Des Devel Ther 2013;7:945–952
54 Zhang L, Dong Z, Liu W, et al. Novel Pharmaceutical strategies for enhancing skin penetration of biomacromolecules. Pharmaceuticals (Basel) 2022;15(07):877
55 Chen YH, Lin DC, Chern E, Huang YY. The use of micro-needle arrays to deliver cells for cellular therapies. Biomed Microdevices 2020;22(04):63
56 Yang H, Kang G, Jang M, et al. Development of lidocaine-loaded dissolving microneedle for rapid and efficient local anesthesia. Pharmaceutics 2020;12(11):1067
57 Yu Q, Huang Y, Zhu C, et al. Combination of microneedles and MF59 adjuvant as a simple approach to enhance transcutaneous immunization. J Biomed Nanotechnol 2020;16(12):1776–1786
58 Dalvi M, Kharat P, Thakor P, Bhavana V, Singh SB, Mehra NK. Panorama of dissolving microneedles for transdermal drug delivery. Life Sci 2021;284:119877
59 Cheng M, Yuan F, Liu J, et al. Fabrication of fine puerarin nanocrystals by Box-Behnken design to enhance intestinal absorption. AAPS PharmSciTech 2020;21(03):90
60 Rouphael NG, Paine M, Mosley R, et al; TIV-MNP 2015 Study Group. The safety, immunogenicity, and acceptability of inactivated influenza vaccine delivered by microneedle patch (TIV-MNP 2015): a randomised, partly blinded, placebo-controlled, phase 1 trial. Lancet 2017;390(10095):649–658
61 Van Damme P, Oosterhuis-Kafeja F, Van der Wielen M, Almagor Y, Sharon O, Levin Y. Safety and efficacy of a novel microneedle device for dose sparing intradermal influenza vaccination in healthy adults. Vaccine 2009;27(03):454–459
62 Chatterjee B, Reddy A, Santra M, Khamanga S. Amorphization of drugs for transdermal delivery-a recent update. Pharmaceutics 2022;14(05):983
63 Yoon DS, Choi Y, Jang Y, et al. SIRT1 directly regulates SOX2 to maintain self-renewal and multipotency in bone marrow-derived mesenchymal stem cells. Stem Cells 2014;32(12):3219–3231
64 Qiang N, Liu Z, Lu M, et al. Preparation and properties of polyvinylpyrrolidone/sodium carboxymethyl cellulose soluble microneedles. Materials (Basel) 2023;16(09):3417
65 Aung NN, Ngawhirunpat T, Rojanarata T, Patrojanasophon P, Opanasopit P, Pamornpathomkul B. HPMC/PVP dissolving microneedles: a promising delivery platform to promote trans-epidermal delivery of alpha-arbutin for skin lightening. AAPS PharmSciTech 2019;21(01):25
66 Wang Q, Yao G, Dong P, et al. Investigation on fabrication process of dissolving microneedle arrays to improve effective needle drug distribution. Eur J Pharm Sci 2015;66:148–156
67 Al-Saidan SM, Krishnaiah YS, Chandrasekhar DV, et al. Formulation of an HPMC gel drug reservoir system with ethanol-water as a solvent system and limonene as a penetration enhancer for enhancing *in vitro* transdermal delivery of nicorandil. Skin Pharmacol Physiol 2004;17(06):310–320
68 Kovačević M, Zvonar Pobirk A, German Ilić I The effect of polymeric binder type and concentration on flow and dissolution properties of SMEDDS loaded mesoporous silica-based granules. Eur J Pharm Sci 2024;193:106582
69 Du H, Liu P, Zhu J, et al. Hyaluronic acid-based dissolving microneedle patch loaded with methotrexate for improved treatment of psoriasis. ACS Appl Mater Interfaces 2019;11 (46):43588–43598
70 Waghule T, Singhvi G, Dubey SK, et al. Microneedles: a smart approach and increasing potential for transdermal drug delivery system. Biomed Pharmacother 2019;109:1249–1258
71 Bala P, Jathar S, Kale S, et al. Transdermal drug delivery system (TDDS)-a multifaceted approach for drug delivery. J Pharm Res 2014;8(12):1805–1835